



Article

A Self-Flux-Biased NanoSQUID with Four NbN-TiN-NbN Nanobridge Josephson Junctions

M. I. Faley *  and R. E. Dunin-Borkowski 

Ernst Ruska-Centre for Microscopy and Spectroscopy with Electrons, Forschungszentrum Jülich GmbH, 52425 Jülich, Germany; r.dunin-borkowski@fz-juelich.de

* Correspondence: m.faley@fz-juelich.de

Abstract: We report the development of a planar 4-Josephson-junction nanoscale superconducting quantum interference device (nanoSQUID) that is self-biased for optimal sensitivity without the application of a magnetic flux of $\Phi_0/4$. The nanoSQUID contains novel NbN-TiN-NbN nanobridge Josephson junctions (nJJs) with NbN current leads and electrodes of the nanoSQUID body connected by TiN nanobridges. The optimal superconducting transition temperature of ~ 4.8 K, superconducting coherence length of ~ 100 nm, and corrosion resistance of the TiN films ensure the hysteresis-free, reproducible, and long-term stability of nJJ and nanoSQUID operation at 4.2 K, while the corrosion-resistant NbN has a relatively high superconducting transition temperature of ~ 15 K and a correspondingly large energy gap. FIB patterning of the TiN films and nanoscale sculpturing of the tip area of the nanoSQUID's cantilevers are performed using amorphous Al films as sacrificial layers due to their high chemical reactivity to alkalis. A cantilever is realized with a distance between the nanoSQUID and the substrate corner of ~ 300 nm. The nJJs and nanoSQUID are characterized using Quantum Design measurement systems at 4.2 K. The technology is expected to be of interest for the fabrication of durable nanoSQUID sensors for low temperature magnetic microscopy, as well as for the realization of more complex circuits for superconducting nanobridge electronics.



Citation: Faley, M.I.; Dunin-Borkowski, R.E. A Self-Flux-Biased NanoSQUID with Four NbN-TiN-NbN Nanobridge Josephson Junctions. *Electronics* **2022**, *11*, 1704. <https://doi.org/10.3390/electronics11111704>

Academic Editor: Antonio Di Bartolomeo

Received: 30 April 2022

Accepted: 24 May 2022

Published: 27 May 2022

Publisher's Note: MDPI stays neutral with regard to jurisdictional claims in published maps and institutional affiliations.



Copyright: © 2022 by the authors. Licensee MDPI, Basel, Switzerland. This article is an open access article distributed under the terms and conditions of the Creative Commons Attribution (CC BY) license (<https://creativecommons.org/licenses/by/4.0/>).

Keywords: titanium nitride; niobium nitride; nanobridge Josephson junction; nanoSQUID; cantilever; superconducting electronics

1. Introduction

The miniaturization of superconducting circuits depends crucially on the implementation of novel Josephson junctions (JJs), including their design and material issues. Progress in applications of superconducting quantum interference devices (SQUIDs), in particular their nanoscale versions (nanoSQUIDs), is critically dependent on the implementation of new JJs. The development of JJs has followed a dialectical Hegel spiral model: the realization of JJs using the tunnel effect [1] has been followed by its observation in superconducting bridges [2], by an improvement in the quality of the tunnel barrier using Nb-Al₂O₃-Nb JJs [3], and by the realization of sub-100 nm Pb nanoSQUIDs with ~ 10 nm nanobridge JJs (nJJs) prepared on a capillary tip [4–6]. Planar nanoSQUIDs with nJJs have been realized using electron beam lithography (see [7] and references therein). The current scale of integration of superconducting circuits of 7.4×10^6 JJs/cm² has been achieved by using a 250-nm-linewidth photolithography process and self-shunted Nb-Al-AlO_x-Nb tunnel JJs with a relatively high J_c of ~ 60 kA/cm² [8]. The critical current densities of nJJs are much higher, with $J_c \sim 1$ MA cm⁻² @ 4.2 K [7], approaching the de-pairing critical current of superconducting films (e.g., ~ 30 MA/cm² for Nb thin films) [9]. High values of $J_c \sim 1$ MA/cm² are required to provide I_c values in the nJJs that are much larger than the thermal noise current $I_{th} = 2\pi k_B T / \Phi_0$ and electromagnetic interference currents in the measurement systems.

The miniaturization of superconducting circuits has to be balanced against the need to squeeze a quantum of magnetic flux into nanoscale superconducting loops containing

JJs: nanoSQUIDs, cells of RSFQ circuits, flux qubits. For 40 nm nanoSQUIDs, the magnetic flux bias of $\Phi_0/4$ that is required for maximal sensitivity corresponds to the application of relatively high magnetic fields of ~ 0.4 T. These fields can influence the magnetic state of an investigated object and suppress T_c of the superconducting film and the JJs of the nanoSQUID itself. The use of control lines or direct injection currents is limited by the critical current of the superconducting films and by small geometrical inductances resulting from the sizes of the nanoSQUIDs [7]. In contrast to geometrical inductance, kinetic and Josephson inductances cannot be used for magnetic flux generation in superconductors because they do not store energy in magnetic fields, but in the form of motion and Josephson energies, respectively. Josephson inductances that are represented by additional Josephson junctions whose critical current I_{c2} is slightly higher than the critical current I_{c1} of the Josephson junctions of the DC SQUID can substitute for flux biasing of nanoSQUIDs without using high magnetic fields. Each Josephson inductance $L(\Delta\varphi) = \Phi_0/2\pi I_c \cos(\Delta\varphi)$, where I_c is the critical current, consumes the phase drop $\Delta\varphi$, reducing the phase drop on the other Josephson junctions, and providing an effective substitution for the magnetic flux bias $\Phi_0/4$ of the nanoSQUID. For this constant shift of the flux voltage characteristics of the nanoSQUID, there is no need for the injection of the additional flux biasing current that was demonstrated for the electrical tuning of a nanoSQUID in [5,6].

Another important issue for nanoscale superconducting components is their long-term stability, which is related to corrosion resistance of the constituent superconducting materials. An extreme example is the high- T_c superconductor $\text{YBa}_2\text{Cu}_3\text{O}_{7-x}$, which degrades so strongly in air [10,11] that the encapsulation of high- T_c SQUIDs in vacuum-tight fiber-glass capsules is required [12]. Thermal cycling of Pb films between a storage temperature of 300 K and an operation temperature of 4.2 K result in hillock and cavity formation on the films, thereby destroying the JJs [13]. Films of the refractory metal Nb are extraordinarily resistant to heat and wear. However, Nb is unstable against corrosion as a result of a reaction with O_2 and H_2O in laboratory air. Oxygen penetrates along grain boundaries from top to bottom in columnar-grown Nb films, producing Nb_2O_5 crystallites that expand and crack the Nb films [14,15]. Oxidation of Nb films can be suppressed significantly by sealing their surface using a hard NbN protection layer, which is stable against H_2 , CO , CO_2 , O_2 , and air [16].

TiN also exhibits excellent corrosion resistance, which is beneficial to the long-term stability of nJJs and nanoSQUIDs [7]. It is used in industry for surface hardening and corrosion protection, as well as for decorative Au-like coatings [17]. Multilayers of NbN/TiN have enhanced mechanical, anticorrosion, and superconducting properties when compared with single-layer NbN and TiN films [18–20]. MoRe is another corrosion-resistant superconducting material that has been used for the preparation of nanoSQUIDs [21,22]. Thin films of NbN and MoRe have relatively large energy gaps $2\Delta \sim 5$ meV. However, their T_c values of up to ~ 16 K and their very short coherence lengths ξ of ~ 5 nm lead to difficulties in the realization of non-hysteretic nanoSQUIDs with nJJs at an operation temperature of 4.2 K [22–24]. nJJs and nanoSQUIDs that are based on nJJs can have hysteretic $I(V)$ characteristics, as a result of (1) the effect of nJJ overheating hysteresis [7,25], or (2) an ambiguity in the $I(\varphi)$ characteristics of nJJs [25,26] in the case of large nJJs when their length is $>3.5 \xi$ [26].

TiN thin films have $T_c \sim 5$ K and $\xi \sim 105$ nm [7,27], which allows the operation of TiN nJJs and nanoSQUIDs without hysteresis at 4.2 K. The absence of hysteresis in the $I(V)$ characteristics near T_c can be explained by an increase in the superconducting coherence length $\xi \propto \left(1 - \frac{T}{T_c}\right)^{-\frac{1}{2}}$ near T_c , according to Ginzburg–Landau theory [28]. Based on the above-mentioned features, it is straightforward to combine the properties of TiN and NbN films in novel NbN-TiN-NbN nJJs that include a TiN nanobridge, NbN electrodes, and current leads to realize non-hysteretic nJJs with a high characteristic voltage $V_c = I_c R_n$, while operating at 4.2 K. The use of such S-S'-S nJJs with NbN as a superconductor with higher T_c (S) and TiN as a superconductor with lower T_c (S') in nanoSQUIDs would improve their voltage response and sensitivity. Pure TiN nJJs and nanoSQUIDs often have $T_c < 4.2$ K,

relatively low values of $\Delta V_{pp} \sim 14 \mu\text{V}$, and a value for the derivative dV/dB of $\sim 44 \mu\text{V}/\Phi_0$ at 4.2 K [7].

Two methods are usually used to pattern nanostructures of TiN, NbN, and Nb: electron beam lithography (EBL) in combination with reactive ion etching (RIE) [7,24,25] and focused ion beam (FIB) milling [25,29]. The high selectivity and isotropy of RIE allow the realization of variable thickness nJJs down to 10 nm resolution [7], but these are sensitive to sample temperature and surface contamination, to the configuration of nearby current leads, and to the granular structure of the etched film, as well as previous processes in the RIE machine: the etch rate of a second sample can then be lower than the etch rate of a first sample. FIB can effectively substitute EBL when there are only few structures such as nanoSQUIDs on a chip and can improve reproducibility, although leading to contamination of the structures by implanted Ga atoms and weakening the heat sink of the nJJs, which can lead to overheating and hysteresis in $I(V)$ characteristics. An auxiliary layer above the superconducting film can provide protection from Ga^+ ions and a better heat sink for each nJJ [28].

Novel NbN-TiN-NbN nJJs and nanoSQUIDs based on such nJJs were prepared using RIE and FIB and are reported in the current paper. For the first time, a low temperature Al sacrificial layer was employed for protection of the superconducting structures against Ga^+ ion implantation during FIB nanofabrication of the nJJs and cantilevers. We realized planar 4-Josephson-junction nanoSQUIDs, which are self-biased to provide optimal sensitivity without the application of high magnetic fields corresponding to the usually required $\Phi_0/4$ magnetic flux bias. The fabrication of cantilevers with a nanoSQUID placed within 300 nm from the substrate corner is also outlined.

2. Materials and Methods

Briefly, 100 nm TiN films covered by 6 nm NbN films were deposited at a rate of $\sim 1 \text{ nm/min}$ from 50 mm 99.95% pure targets using pulsed reactive DC magnetron sputtering onto Si (001) substrates that were heated to $\sim 800^\circ\text{C}$. The substrates were cleaned one after the other in an ultrasonic bath in acetone, propanol, and deionized water and etched with an Ar^+ ion beam just before placing them in a home-built sputtering machine, which was evacuated to a base pressure of $< 4 \times 10^{-8} \text{ mbar}$ using oil-free pumps. Deposition was performed in an $\text{Ar}(80\%)\text{-N}_2(20\%)$ gas mixture at a total pressure of 10^{-2} mbar . A N_2 flow of 5 ml/min was regulated using a Brooks© mass flow controller 5850 TR. The Ar and N_2 gases had a purity of 99.9999% and contained less than 0.01 ppm O_2 , which corresponds to an O_2 partial pressure of less than 10^{-10} mbar . Before deposition, the chamber was outgassed at the deposition conditions during pre-sputtering onto the closed shutter for more than 1 h.

The nanoSQUID design included 4 nJJs with 2 critical currents $I_{c1} < I_{c2}$ and 3 current leads, as shown schematically in Figure 1.

TiN-NbN heterostructures were patterned using EBL in combination with RIE using masks of diluted AZ nLOF 2020 electron beam resist and/or by FIB. The resist was exposed using an electron beam with an accelerating voltage of 100 kV, a current of 10 nA, and a dose of $120 \mu\text{C}/\text{cm}^2$. RIE of the TiN-NbN heterostructures was performed using a pure SF_6 atmosphere, which resulted in isotropic etching of both the NbN and the TiN films at a rate of $\sim 1 \text{ nm/s}$ with a selectivity of ~ 3 for etching of TiN-NbN heterostructures relative to the diluted nLOF 2020 resist. After RIE, resist residuals were removed from the samples by soaking in warm acetone at 70°C and in distilled water. Figure 2 shows (a) a schematic representation and (b) a scanning electron microscopy (SEM) image of the resulting NbN-TiN-NbN nJJs. Thanks to the undercut due to isotropic etching, the top layer of the NbN is locally removed in the nanobridge area. The electrodes contain the TiN-NbN heterostructures, where the energy gap of TiN is enhanced by a proximity effect from the NbN layer. Pieces of In of size $\sim (0.5 \text{ mm})^3$ were used to form galvanic contacts to the structures through the Si passivation layer.

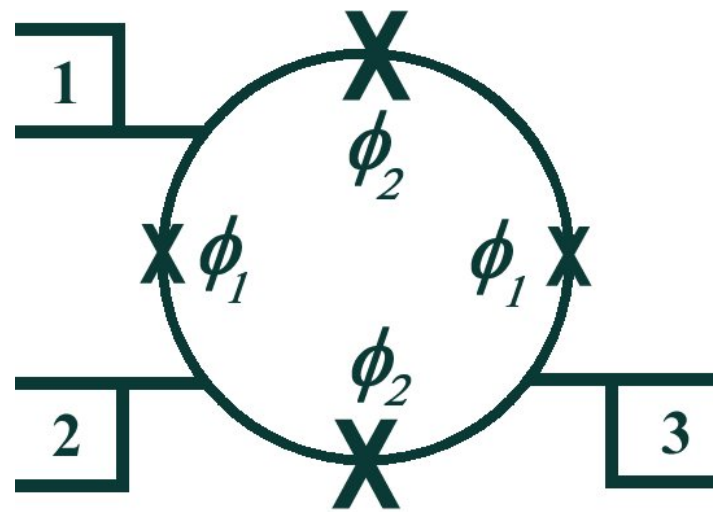


Figure 1. Schematic diagram of a 4 nJJ nanoSQUID with 3 current leads. Josephson junctions with larger critical currents I_{c2} and smaller phase drops $\phi_2 < \pi/2$ are shown by larger crosses.

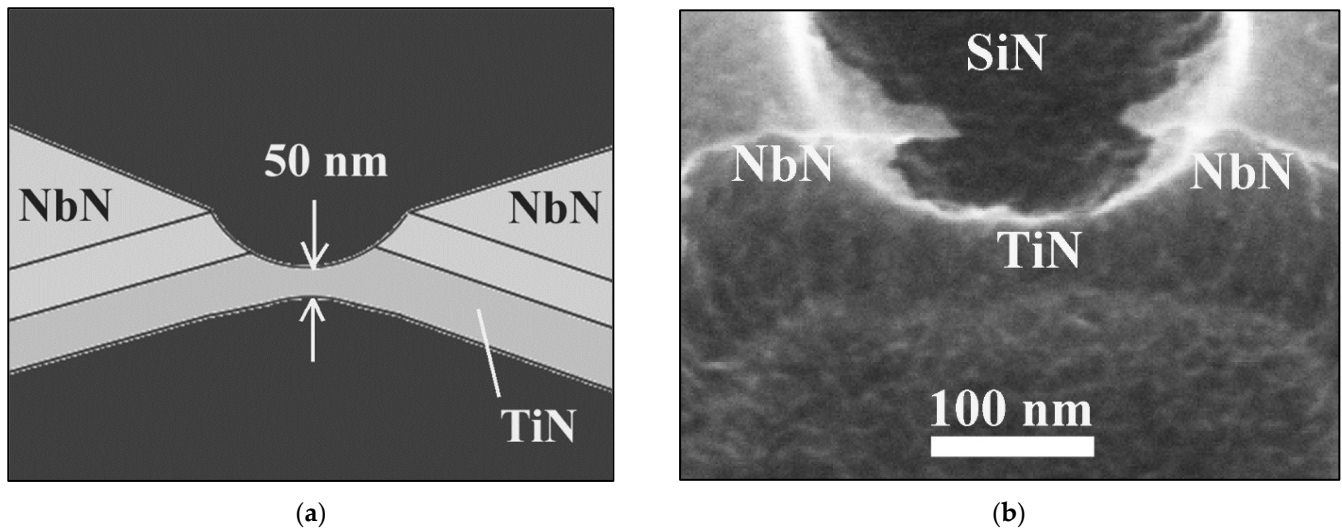


Figure 2. (a) Schematic view of a NbN-TiN-NbN nJJ. (b) SEM image of a NbN-TiN-NbN nJJ prepared using RIE. The image was recorded at an accelerating voltage of 15 kV and a sample tilt angle of 45° .

When performing FIB etching of the nJJs, the structures were covered by a >100-nm-thick protection layer of amorphous Al that was deposited at 77 K to reduce the size of the grains in the Al film to a negligible value of ~ 1 nm. A dual-beam FEI Helios NanoLab 400S FIB system was used with Ga^+ ions at an accelerating voltage of 30 kV and a current of 1.5 pA to etch a $300 \text{ nm} \times 300 \text{ nm}$ hole and form 4 nJJs. An additional 100-nm-thick amorphous Si layer was deposited at room temperature above the nanoSQUID to provide a better thermal shunt of the nJJs. For bulk nanomachining of cantilevers with nanoSQUIDs, the Al protection layer was up to $\sim 1.5 \mu\text{m}$ thick, which allowed for the use of the maximal available Ga^+ focused ion beam of ~ 21 nA. After FIB, the Al layer and the fences of redeposited material were removed by chemical etching of Al using an AZ 726 MIF developer in an ultrasonic bath.

The microstructures of the films, nJJs, and nanoSQUIDs were investigated using high-resolution scanning electron microscopy (HRSEM) in a Zeiss 1550 VP. $R(T)$ dependences of the TiN and NbN films and TiN-NbN heterostructures were recorded using Quantum Design (QD) Physical Property Measurement Systems (PPMS). $R(T)$ and $I(V)$ characteristics of the nJJs and nanoSQUIDs were measured using a QD DynaCool system. Voltage

modulations of the nanoSQUIDs with magnetic field $V(B)$ at different current biases and temperatures were measured using the PPMS.

3. Results

The deposition of a NbN film above a TiN film significantly improved the superconducting properties of the NbN films: the T_c value of 60-nm-thick NbN films increased from 10.6 to 14.5 K and the residual resistance ratio (RRR) R_{300K}/R_{10K} increased from 0.9 to 2.4 when compared to NbN films deposited under the same conditions on pristine Si (100) substrates. Resistivity values of $\sim 6 \mu\Omega\cdot\text{cm}$ at room temperature and $\sim 7 \mu\Omega\cdot\text{cm}$ at 10 K were measured for the NbN films. The latter value is close to values of $\sim 5 \mu\Omega\cdot\text{cm}$ at 10 K obtained for TiN films deposited on oxide-free Si at 800 °C [7,30], which is advantageous for the proximity effect between NbN and TiN films: the small difference between the specific resistances and the large coherence length in TiN result in a value of $\gamma \sim 0.01$ in Refs. [31,32], which corresponds to negligibly small suppression of the superconducting order parameter in the layers due to the proximity effect and a small jump in the order parameter at the interlayer boundary due to the interface resistance. The superconducting transition temperature T_c of the NbN-TiN heterostructures depends on the thickness of the NbN layer and is ~ 6 K for a 6 nm NbN layer above a 100-nm-thick TiN film. A lower base pressure of $\leq 4 \times 10^{-8}$ mbar and a higher substrate temperature of ≥ 800 °C lead to a higher value of T_c . The observed RRR value of >2 reflects a relatively long mean free path of the charge carriers in NbN-TiN heterostructures due to a relatively low concentration of defects.

A similar improvement in the electron transport properties of NbN films deposited on Si substrates buffered by TiN was observed in [30] and attributed to the improved crystallinity of NbN films grown epitaxially on TiN films: the size of grains in NbN films grown directly on Si would be smaller than the size of grains in TiN films also grown directly on Si because of the lower mobility of Nb atoms. Figure 3 shows an SEM image of a cross-section of a NbN-TiN heterostructure grown on a pristine Si (001) substrate and contains a much thicker NbN layer than it was used for nJJs and nanoSQUIDs. The image was recorded at an accelerating voltage of 30 kV with the sample broken parallel to a Si (110) plane that was perpendicular to the film surface. This image demonstrates the continuity of grains across the interface boundary, in accordance with the epitaxial growth of NbN on TiN. In Figure 3, the grains in the NbN layer look larger and are slightly lighter than the grains in the TiN layer.

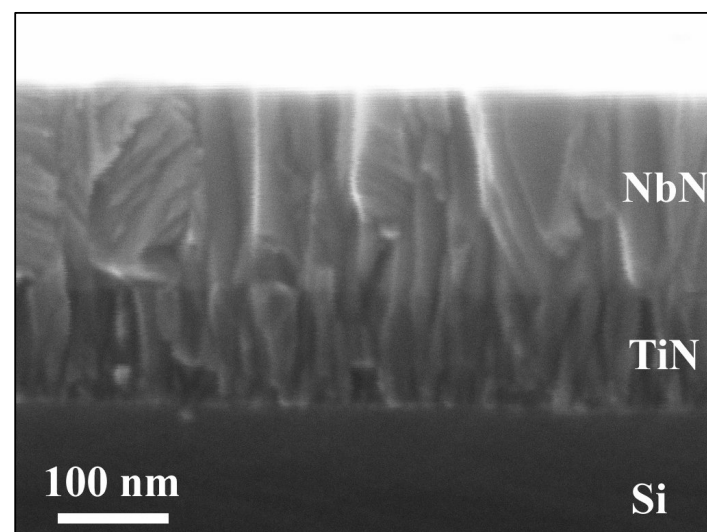


Figure 3. SEM image of a cross-section of a NbN-TiN heterostructure on a Si (001) substrate. The image was recorded with the sample broken parallel to a Si (110) plane perpendicular to the film surface.

The patterning of superconducting nanostructures using FIB is a very attractive alternative to RIE because it provides better control of geometrical dimensions of the nJJs. Figure 4 shows an SEM image of a nanoSQUID that was made using FIB etching with four 50-nm-long nJJs, a $300\text{ nm} \times 300\text{ nm}$ hole, and three current leads, in accordance with the schematic representation shown in Figure 1. The nanoSQUID was covered by a 100-nm-thick protection layer of Al, which was sputtered on the sample at 77 K. (Films of Al deposited at room temperature contained large grains up to 100 nm in size, which disturbed the SEM view and FIB etching). Focusing and correction of astigmatism in the FIB was complicated by the weak secondary electron image when using the smallest current of the Ga^+ ion beam of $\sim 1.5\text{ pA}$ for patterning the nJJs and requires further optimization.

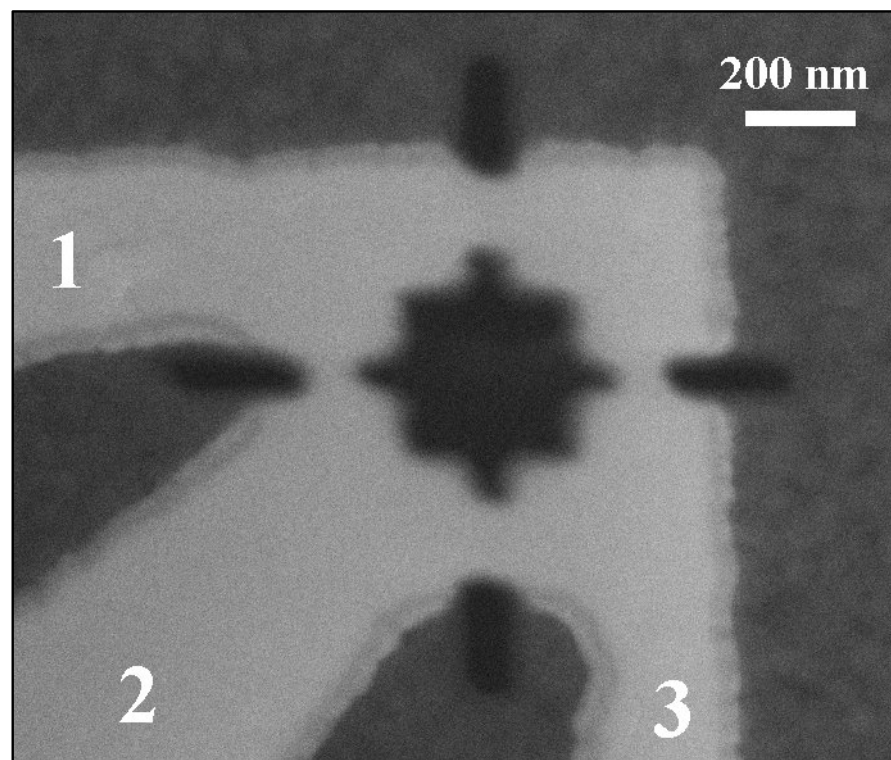


Figure 4. SEM image of a nanoSQUID fabricated using FIB etching with four $\sim 50\text{-nm}$ -long nJJs, a $300\text{ nm} \times 300\text{ nm}$ hole and 3 current leads, in accordance with the schematic diagram shown in Figure 1.

FIB was tested for the preparation of a nanoSQUID cantilever tip as an alternative method to the mechanical and RIE techniques described in ref. [33]. A protection Al layer deposited at 77 K $\sim 1.5\text{ }\mu\text{m}$ thick allows to position, focus, and perform the etching using maximal available current $\sim 21\text{ nA}$ of the focused Ga^+ ion beam. The material volume per dose rate is $\sim 0.3\text{ }\mu\text{m}^3/\text{nC}$ at an accelerating voltage of 30 kV for Si and Al, which allows a $5\text{ }\mu\text{m} \times 100\text{ }\mu\text{m} \times 50\text{ }\mu\text{m}$ slit to be cut in $\sim 1\text{ h}$. Pre-thinning of the nanoSQUID cantilever chip down to a thickness of $\sim 50\text{ }\mu\text{m}$ can be performed using ICP RIE [33] or chemical etching in 20% KOH solution [7]. By using FIB, we succeeded to position a nanoSQUID within 100 nm from the substrate corner. Based on safety and resolution considerations for the lateral outer dimension of the nanoSQUID of $\sim 900\text{ nm}$ and the total thickness of the superconducting film of the nanoSQUID of up to $\sim 200\text{ nm}$, it is optimal to place the nanoSQUID at a distance of $\sim 300\text{ nm}$ from the edges of the substrate (see Figure 5). The corner can then be used as the tip of a cantilever when it is placed at a small angle of $\sim 10^\circ$ relative to the surface of an investigated magnetic object.

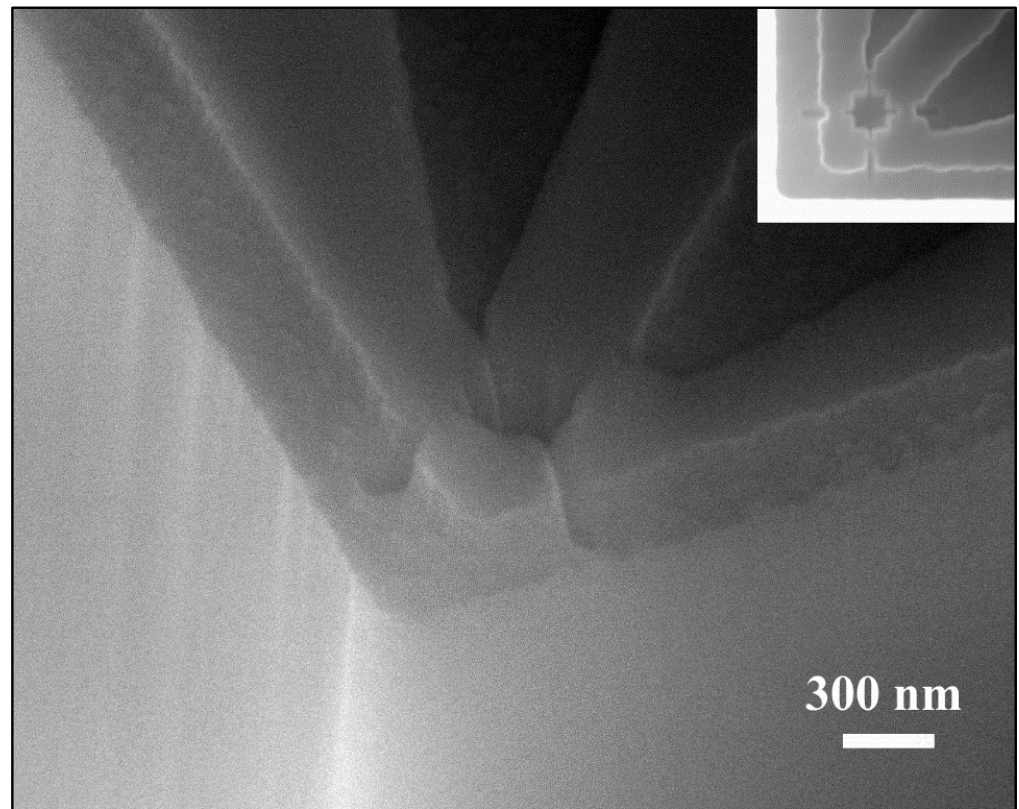


Figure 5. HRSEM image of a Si cantilever with a 4JJ nanoSQUID placed within 300 nm of the corner by FIB etching. The inset shows a top view of the same nanoSQUID cantilever.

Despite the implementation of 100-nm-thick protection layers of Al, a deterioration in the superconducting parameters of the nJJs was observed (the operation temperature dropped below 4.2 K for pure TiN), as well as for S-S'-S nJJs (where for FIB-prepared nJJs the NbN-TiN heterostructure in the S' nanobridge is damaged at the top NbN layer and on the sides of the nJJs by implanted Ga atoms). This effect is smaller if a thicker protection layer is used during FIB milling of the nJJs but could not be completely avoided. Implanted Ga penetrates the films much deeper than 30 nm, as suggested in [25] for an accelerating voltage of 25 kV, and probably causes a larger deteriorating effect on NbN and TiN films than on the Nb films described in [25]. The preparation of nJJs using FIB patterning should be further optimized to reduce Ga⁺ ion implantation, e.g., by the use of thicker protection layers.

RIE allows patterning of nJJs that are free from the contamination that currently results in a higher value of T_c by ~ 0.4 K and a larger characteristic voltage $V_c = I_c R_n$ by ~ 4 times of the nJJs, when compared with nJJs that were prepared from similar NbN-TiN heterostructures using FIB. The NbN layer was removed in the middle of the nJJs by undercutting during the isotropic RIE process (see Figure 2), resulting in the formation of variable thickness nanobridge NbN-TiN-NbN JJs. RIE was performed at 25 W with 5 Pa of pure SF₆ gas, providing an etch rate of ~ 1 nm/s normal to the surface of the NbN-TiN heterostructure and an undercut in-plane etching rate of ~ 0.3 nm/s, which provides a relationship between the optimal width of the bridges in the e-beam resist and the thickness of the NbN-TiN heterostructure. However, there is a significant dependence of the RIE rate in SF₆ gas on sample surface cleanliness and on the prehistory of operation of the RIE machine. Contamination of the sample surface and the chamber hinders reactive etching. In order to ensure reproducibility of the nJJs, the RIE machine was cleaned and preconditioned prior to the installation of the substrates. The substrates lay freely on a quartz plate whose temperature was maintained at 20 °C. Moderate heating of the substrate during RIE increases the etch rate and should be taken into account. After RIE, residuals of

the nLOF resist were removed in warm acetone and did not disturb the establishment of galvanic contacts to successive Pt, Au, and bulk In layers on the contact pads.

Figure 6 shows the $I(V)$ dependences of a 4JJ-nanoSQUID that contains two ~ 30 -nm-wide and two ~ 50 -nm-wide NbN-TiN-NbN nJJs patterned using RIE and characterized at 4.2 K. The critical current of the nanoSQUID depends on the magnetic field from a minimal value of $\sim 25 \mu\text{A}$ at 10 G to a maximal critical current of $\sim 39 \mu\text{A}$ at -30 G. The $I(V)$ characteristics are non-hysteretic, despite the relatively large critical currents and characteristic voltage $V_c = I_c R_n \cong 200 \mu\text{V}$.

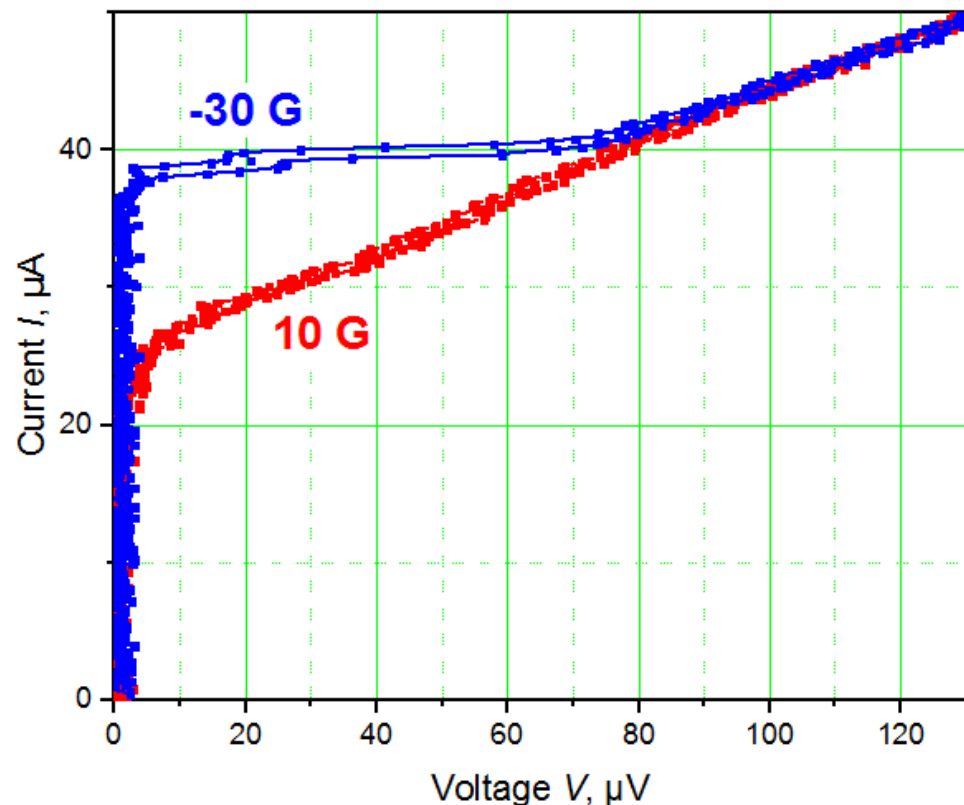


Figure 6. $I(V)$ dependences measured for a planar nanoSQUID with NbN-TiN-NbN junctions in magnetic fields of -30 G (blue) and 10 G (red) at 4.2 K.

At bias currents between ~ 25 and $\sim 45 \mu\text{A}$, the voltage on the nanoSQUID depends periodically on the external field normal to the nanoSQUID's plane with a period of ~ 60 G. The $V(B)$ dependence of the nanoSQUID at 4.2 K measured using a bias current $I_c = 39 \mu\text{A}$ is shown in Figure 7. The observed large amplitude of the voltage modulation $\Delta V_{p-p} \sim 50 \mu\text{V}$ (peak-to-peak) is due to the presence of the NbN film in the electrodes and the relatively low kinetic inductance of the nanoSQUID, which is based on Josephson junctions in the form of nanobridges of variable thickness: the washer of the nanoSQUID is much thicker than in Dayem bridges. The 60 G period of the modulation corresponds to an effective area of $0.36 \mu\text{m}^2$ of the nanoSQUID. Thanks to the 4JJ design, the nanoSQUID does not require flux biasing: At 0 G, the derivative dV/dB has already reached its maximal value of $\sim 525 \mu\text{V}/\Phi_0$.

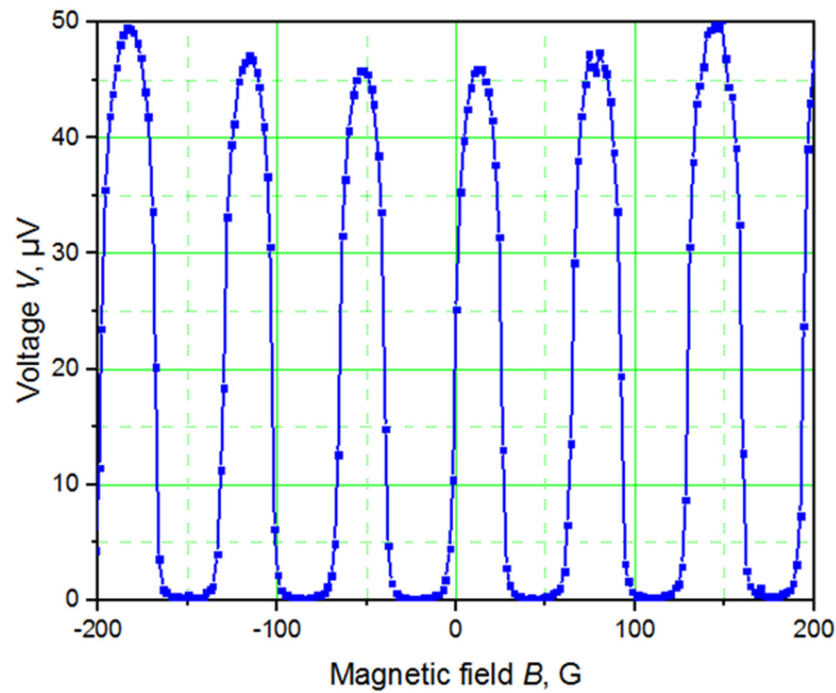


Figure 7. $V(B)$ curve of the planar nanoSQUID with NbN-TiN-NbN nJJs measured with a bias current of 39 μA at 4.2 K.

4. Discussion

The proposed design of a 4-nJJ nanoSQUID (Figure 1) provides a solution to the problem of $\Phi_0/4$ magnetic flux bias of nanoSQUID to the maximum responsivity point at which the derivative of the SQUID voltage with magnetic field dV/dB has a maximal value. The operation principle of such a 4-nJJ nanoSQUID is as follows. The magnetic flux Φ through the loop of the nanoSQUID connected with the phase drops φ_1 and φ_1 across the nJJs according to equation

$$2\varphi_1 + 2\varphi_2 + 2\pi\Phi/\Phi_0 = 2\pi n, \quad (1)$$

where n is an integer. The bias current of the nanoSQUID is $I_b = 2I_{c1}\sin\varphi_1 \cong 2I_{c1}$. The junctions with the largest phase drop φ_1 have the smallest critical current I_{c1} , which is reached at $\varphi_1 = \pi/2$. Each of the other two junctions has a phase drop φ_2 determined by their maximal current, which is limited by the critical current of the smallest junctions I_{c1} and its critical current I_{c2} : $\varphi_2 = \arcsin(I_{c1}/I_{c2})$. This maximal current is reached when the magnetic flux through the nanoSQUID is $\Phi = (\pi n - \pi/2 - \varphi_2) \cdot \Phi_0/\pi$. The maximum responsivity point in zero external magnetic field is when this magnetic flux $\Phi = \Phi_0/4$: $2\pi/2 + 2\varphi_2 + 2\pi/4 = 2\pi n$, or:

$$\varphi_2 = \pi n - \pi/2 - \pi/4 \quad (2)$$

Equation (2) determines, to a first approximation, the relationship between the critical currents: $I_{c2} = I_{c1}/\sin(\pi/4) = I_{c1}\sqrt{2}$ at $n = 1$. The true optimal critical current I_{c2} differs from the calculated value because the geometrical inductances of the nJJs are not zero and spread of dimensions of the nJJs should also be taken into account. An asymmetric DC SQUID that contains two nJJs with different critical currents can be used for self-flux-biasing [34]. If the size of the SQUID loop is $>1 \mu\text{m}$, then the geometrical inductance of the SQUID loop can also be used for the creation of self-biasing, e.g., in a 3-JJ SQUID configuration [35]. However, these alternative methods are less effective when the size of the SQUIDs is on the nm scale and the geometrical inductances of the nJJs and of the SQUID loop become negligible.

In addition, one should take into account the fact that Ginzburg–Landau theory describes the Josephson effect in nanobridges only in close proximity to T_c , where the coherence length is comparable with the dimensions of the nJJs [26,28,36,37]. For real nJJs, the largest voltage modulation is observed in proximity to hysteretic $I(V)$ characteristics, where theoretical models partially deviate from experimentally observed properties (e.g., the current-phase relationship of nJJs deviates from a sinusoidal form).

The comparison of two patterning techniques performed in the present study has illustrated their respective advantages and disadvantages for the preparation of NbN–TiN–NbN nanobridges and self-flux-biased nanoSQUIDs. FIB milling offers adequate spatial resolution for the reproducible structuring of NbN–TiN–NbN nJJs but contaminates films with Ga, thereby deteriorating their superconducting properties. A sufficiently thick protection layer of Al deposited at 77 K reduces this contamination and allows the nanoSQUID to be placed within ~ 100 nm of the substrate edge, which is essential for the preparation of a cantilever. Although optimization of the protection layer for the preparation of nanoSQUIDs by FIB seems to be promising, the best results are currently obtained using RIE.

The noise level of the nanoSQUID-based measurement system is determined mainly by the white noise input level $\sqrt{S_v} \sim 1$ nV/ $\sqrt{\text{Hz}}$ of the preamplifier at room temperature [7]. The magnetic flux resolution of the present measurement system $\sqrt{S_\Phi} \cong \sqrt{S_v}/(\partial V/\partial \Phi) \sim 1.9 \mu\Phi_0/\sqrt{\text{Hz}}$, where the derivative $\partial V/\partial \Phi \cong 525 \mu\text{V}/\Phi_0$. For comparison with other planar nanoSQUIDs, flux noise values of $1.7 \mu\Phi_0/\sqrt{\text{Hz}}$ [22] and $0.3 \mu\Phi_0/\sqrt{\text{Hz}}$ [23] have been achieved for nanoSQUIDs with hysteretic $I(V)$ characteristics measured at temperatures of $\ll T_c$. By increasing the thickness of the NbN layer, nanoSQUIDs with NbN–TiN–NbN nJJs also become hysteretic in their $I(V)$ characteristics. The study of measurement systems with hysteretic nanoSQUIDs is beyond the scope of the present work.

5. Conclusions

We have tested NbN–TiN–NbN nJJs and planar 4-JJ nanoSQUIDs that were prepared using FIB and RIE. The planar 4-JJ nanoSQUIDs are self-biased for optimal sensitivity without the application of magnetic flux of $\Phi_0/4$. The nanoSQUIDs contain novel NbN–TiN–NbN nanobridge Josephson junctions (nJJs), with NbN electrodes connected by TiN nanobridges. TiN has an optimal superconducting transition temperature of ~ 4.8 K, a superconducting coherence length of ~ 100 nm, and corrosion resistance, offering hysteresis-free, reproducible, and long-term stability for nJJ and nanoSQUID operation at 4.2 K, while corrosion-resistant NbN has a relatively high superconducting transition temperatures up to ~ 16 K and a correspondingly large energy gap. FIB patterning of TiN films and nanoscale sculpturing of the tip area of the nanoSQUID's cantilevers were performed by using amorphous Al films as sacrificial layers due to their relatively high chemical reactivity to alkalis. A cantilever with a distance between the nanoSQUID and the substrate corner of ~ 300 nm was realized. The $I(V)$ characteristics of the nJJs and nanoSQUIDs, as well as the voltage modulation of the nanoSQUIDs, was measured at 4.2 K. The developed technology can be used for the fabrication of durable nanoSQUID sensors for low temperature magnetic microscopy, as well as for the realization of more complex circuits for superconducting nanobridge electronics.

Author Contributions: Conceptualization, methodology and original draft preparation, M.I.F.; investigation, formal analysis, data curation, M.I.F.; supervision and resources, M.I.F. and R.E.D.-B. All authors contributed to the review and editing of the manuscript, as well reading and agreeing to the published version of the manuscript. All authors have read and agreed to the published version of the manuscript.

Funding: This research received no external funding.

Informed Consent Statement: Not applicable.

Acknowledgments: The authors gratefully acknowledge R. Borowski, L. Kibkalo, H. Stumpf, M. Nonn, S. Trellenkamp, F. Lentz, E. Neumann, O. Petravic, S. Nandi, B. Schmitz and G. Potemkin for technical assistance.

Conflicts of Interest: The authors declare no conflict of interest.

References

- Giaever, I.; Megerle, K. Study of Superconductors by Electron Tunneling. *Phys. Rev.* **1961**, *122*, 1101–1111. [\[CrossRef\]](#)
- Anderson, P.W.; Dayem, A.H. Radio-Frequency Effects in Superconducting Thin Film Bridges. *Phys. Rev. Lett.* **1964**, *13*, 195–197. [\[CrossRef\]](#)
- Gurvitch, M.; Washington, M.A.; Huggins, H.A. High quality refractory Josephson tunnel junctions utilizing thin aluminum layers. *Appl. Phys. Lett.* **1983**, *42*, 472–474. [\[CrossRef\]](#)
- Vasyukov, D.; Anahory, Y.; Embon, L.; Halbertal, D.; Cuppens, J.; Neeman, L.; Finkler, A.; Segev, Y.; Myasoedov, Y.; Rappaport, M.L.; et al. A scanning superconducting quantum interference device with single electron spin sensitivity. *Nat. Nanotechnol.* **2013**, *8*, 639–644. [\[CrossRef\]](#) [\[PubMed\]](#)
- Uri, A.; Meltzer, A.Y.; Anahory, Y.; Embon, L.; Lachman, E.O.; Halbertal, D.; Hr, N.; Myasoedov, Y.; Huber, M.E.; Young, A.F.; et al. Electrically Tunable Multiterminal SQUID-on-Tip. *Nano Lett.* **2016**, *16*, 6910–6915. [\[CrossRef\]](#) [\[PubMed\]](#)
- Meltzer, A.Y.; Uri, A.; Zeldov, E. Multi-terminal multi-junction dc SQUID for nanoscale magnetometry. *Supercond. Sci. Technol.* **2016**, *29*, 114001. [\[CrossRef\]](#)
- Faley, M.I.; Fiadziushkin, H.; Frohn, B.; Schüffegen, P.; Dunin-Borkowski, R.E. TiN nanobridge Josephson junctions and nanoSQUIDs on SiN-buffered Si. *Supercond. Sci. Technol.* **2022**, *35*, 065001. [\[CrossRef\]](#)
- Tolpygo, S.K.; Semenov, V.K. Increasing integration scale of superconductor electronics beyond one million Josephson junctions. *J. Phys. Conf. Ser.* **2020**, *1559*, 012002. [\[CrossRef\]](#)
- Il'in, K.; Rall, D.; Siegel, M.; Engel, A.; Schilling, A.; Semenov, A.; Huebers, H.-W. Influence of thickness, width and temperature on critical current density of Nb thin film structures. *Phys. C Supercond.* **2010**, *470*, 953–956. [\[CrossRef\]](#)
- Zhao, R.; Myhra, S. Environmental degradation of YBa₂Cu₃O_{7-x} A descriptive and predictive model. *Phys. C Supercond.* **1994**, *230*, 75–81. [\[CrossRef\]](#)
- Regier, M.; Keskin, E.; Halbritter, J. Corrosion of superconductors: Especially of YBa₂Cu₃O_{7-δ} cuprate. *IEEE Trans. Appl. Supercond.* **1999**, *9*, 2375. [\[CrossRef\]](#)
- Faley, M.I.; Poppe, U.; Urban, K.; Paulson, D.N.; Starr, T.; Fagaly, R.L. Low noise HTS dc-SQUID flip-chip magnetometers and gradiometers. *IEEE Trans. Appl. Supercond.* **2001**, *11*, 1383–1386. [\[CrossRef\]](#)
- Lahiri, S.K. Metallurgical considerations with respect to electrodes and interconnection lines for Josephson tunneling circuits. *J. Vac. Sci. Technol.* **1976**, *13*, 148–151. [\[CrossRef\]](#)
- Halbritter, J. ARXPS analysis and oxidation of niobium compounds. *Electrochim. Acta* **1989**, *34*, 1153–1155. [\[CrossRef\]](#)
- Halbritter, J. Transport in superconducting niobium films for radio frequency applications. *J. Appl. Phys.* **2005**, *97*, 083904. [\[CrossRef\]](#)
- Isagawa, S. rf superconducting properties of reactively sputtered NbN. *J. Appl. Phys.* **1981**, *52*, 921–927. [\[CrossRef\]](#)
- Vershinin, N.; Filonov, K.; Straumal, B.; Gust, W.; Wiener, I.; Rabkin, E.; Kazakeviche, A. Corrosion behaviour of the protective and decorative TiN coatings on large area steel strips. *Surf. Coat. Technol.* **2000**, *125*, 229–232. [\[CrossRef\]](#)
- Sugumaran, A.A.; Purandare, Y.; Shukla, K.; Khan, I.; Ehasarian, A.; Hovsepian, P. TiN/NbN Nanoscale Multilayer Coatings Deposited by High Power Impulse Magnetron Sputtering to Protect Medical-Grade CoCrMo Alloys. *Coatings* **2021**, *11*, 867. [\[CrossRef\]](#)
- Barshilia, H.C.; Prakash, M.S.; Poojari, A.; Rajam, K.S. Corrosion behavior of nanolayered TiN/NbN multilayer coatings prepared by reactive direct current magnetron sputtering process. *Thin Solid Film.* **2004**, *460*, 133–142. [\[CrossRef\]](#)
- Zhang, J.J.; Su, X.; Zhang, L.; Zheng, L.; Wang, X.F.; You, L. Improvement of the superconducting properties of NbN thin film on single-crystal silicon substrate by using a TiN buffer layer. *Supercond. Sci. Technol.* **2013**, *26*, 045010. [\[CrossRef\]](#)
- Bagani, K.; Sarkar, J.; Uri, A.; Rappaport, M.L.; Huber, M.E.; Zeldov, E.; Myasoedov, Y. Sputtered Mo 66 Re 34 SQUID-on-Tip for High-Field Magnetic and Thermal Nanoimaging. *Phys. Rev. Appl.* **2019**, *12*, 044062. [\[CrossRef\]](#)
- Shishkin, A.G.; Skryabina, O.V.; Gurtovoi, V.L.; Dizhur, S.E.; Faley, M.I.; Golubov, A.A.; Stolyarov, V.S. Planar MoRe-based direct current nanoSQUID. *Supercond. Sci. Technol.* **2020**, *33*, 065005. [\[CrossRef\]](#)
- Russo, R.; Esposito, E.; Crescitelli, A.; Di Gennaro, E.; Granata, C.; Vettoliere, A.; Cristiano, R.; Lisitskiy, M. NanoSQUIDs based on niobium nitride films. *Supercond. Sci. Technol.* **2017**, *30*, 024009. [\[CrossRef\]](#)
- Holzman, I.; Ivry, Y. On-chip integrable planar NbN nanoSQUID with broad temperature and magnetic-field operation range. *AIP Adv.* **2019**, *9*, 105028. [\[CrossRef\]](#)
- Troeman AG, P.; Derking, H.; Borger, B.; Pleikies, J.; Veldhuis, D.; Hilgenkamp, H. NanoSQUIDs Based on Niobium Constrictions. *Nano Lett.* **2007**, *7*, 2152–2156. [\[CrossRef\]](#)
- Likharev, K.K. Superconducting weak links. *Rev. Mod. Phys.* **1979**, *5*, 101–159. [\[CrossRef\]](#)
- Faley, M.I.; Liu, Y.; Dunin-Borkowski, R.E. Titanium Nitride as a New Prospective Material for NanoSQUIDs and Superconducting Nanobridge Electronics. *Nanomaterials* **2021**, *11*, 466. [\[CrossRef\]](#)

28. Tinkham, M. *Introduction to Superconductivity*, 2nd ed.; McGraw-Hill: New York, NY, USA, 1996; ISBN 0486435032.
29. Patel, T.; Li, B.; Gallop, J.; Cox, D.; Kirkby, K.; Romans, E.; Chen, J.; Nisbet, A.; Hao, L. Investigating the Intrinsic Noise Limit of Dayem Bridge NanoSQUIDs. *IEEE Trans. Appl. Supercond.* **2015**, *25*, 1602105. [[CrossRef](#)]
30. Sun, R.; Makise, K.; Qiu, W.; Terai, H.; Wang, W. Fabrication of (200)-Oriented TiN Films on Si (100) Substrates by DC Magnetron Sputtering. *IEEE Trans. Appl. Supercond.* **2015**, *25*, 1101204. [[CrossRef](#)]
31. Kupriyanov, M.Y.; Likharev, K.K. Towards the quantitative theory of the high-T/sub c/Josephson junctions. *IEEE Trans. Magn.* **1991**, *27*, 2460–2463. [[CrossRef](#)]
32. Golubov, A.A.; Houwman, E.P.; Gijssbertsen, J.G.; Krasnov, V.M.; Flokstra, J.; Rogalla, H.; Kupriyanov, M.Y. Proximity effect in superconductor-insulator-superconductor Josephson tunnel junctions: Theory and experiment. *Phys. Rev. B* **1995**, *51*, 1073–1089. [[CrossRef](#)] [[PubMed](#)]
33. Faley, M.I.; Bikulov, T.; Bosboom, V.; Golubov, A.A.; Dunin-Borkowski, R.E. Bulk nanomachining of cantilevers with Nb nanoSQUIDs based on nanobridge Josephson junctions. *Supercond. Sci. Technol.* **2021**, *34*, 035014. [[CrossRef](#)]
34. Muller, J.; Weiss, S.; Gross, R.; Kleiner, R.; Koelle, D. Voltage-flux-characteristics of asymmetric dc SQUIDs. *IEEE Trans. Appl. Supercond.* **2001**, *11*, 912–915. [[CrossRef](#)]
35. Neeley, M.; Ansmann, M.; Bialczak, R.C.; Hofheinz, M.; Katz, N.; Lucero, E.; O’Connell, A.; Wang, H.; Cleland, A.N.; Martinis, J.M. Transformed dissipation in superconducting quantum circuits. *Phys. Rev. B* **2008**, *77*, 180508. [[CrossRef](#)]
36. Aslamazov, L.G.; Larkin, A.I. Josephson effect in superconducting point contacts. *ZhETF Pisma Redaktsiiu* **1968**, *9*, 150–154.
37. Schmidt, V.V. *The Physics of Superconductors*; Müller, P., Ustinov, A.V., Eds.; Springer: Berlin/Heidelberg, Germany, 1997; ISBN 978-3-642-08251-1. [[CrossRef](#)]